Mid-infrared refractive index sensing using optimized slotted photonic crystal waveguides

Lazhar Kassa-Baghdouche, Eric Cassan

Photonics and Nanostructures - Fundamentals and Applications 28, 32-36 (2018).

Mid-infrared refractive index sensing using optimized slotted photonic crystal waveguides

Lazhar Kassa-Baghdouche[a,*], Eric Cassan[b]

[a] *Département d'Electronique et de Télécommunications, Faculté des Sciences et de la Technologie, Université 8 Mai 1945, Guelma 24000, Algeria*
[b] *Centre de Nanosciences et de Nanotechnologies, CNRS, Université Paris-Sud, Université Paris-Saclay, C2N - Orsay, 91405 Orsay cedex, France*

Abstract

Slotted photonic crystal waveguides (SPCW) were designed to act as refractive index sensing devices at mid-infrared (IR) wavelengths around $\lambda = 3.6\ \mu m$. In particular, effort was made to engineer the input and output slot waveguide interfaces in order to increase the effective sensitivity through resonant tapering. A slotted PhC waveguide immersed in air and liquid cladding layers was considered. To determine the performance of the sensor, the sensitivity of the device was estimated by calculating the shift in the upper band edge of the output transmission spectrum. The results showed that the sensitivity of a conventionally designed SPCW followed by modifications in the structure parameter yielded a 510 nm shift in the wavelength position of the upper band edge, indicating a sensitivity of more than 1150 nm per refractive index unit (RIU) with an insertion loss level of -0.3 dB. This work demonstrates the viability of photonic crystal waveguide high sensitivity devices in the Mid-IR, following a transposition of the concepts inherited from the telecom band and an optimization of the design, in particular a minimization of photonic device insertion losses.

Keywords: `Mid-infrared, Slotted photonic crystal waveguides, Resonators structures, Refractive index sensor, Photonic crystals`

∗. Corresponding author : Lazhar Kassa-Baghdouche
Email address: `kassabaghdouche_lazhar@yahoo.com` (Lazhar Kassa-Baghdouche)

Preprint submitted to Photonics and Nanostructures: Fundamentals and Applications 6 octobre 2017

1. Introduction

There has been considerable focus on silicon photonics in the last several years, largely owing to its applications in near-IR data communications in the telecommunication wavelength band. However, silicon is also optically transparent in the wavelength range between 1.1 μm and 8 μm. Therefore, it offers a range of uses in environmental and biochemical sensing [1]. Conversely, because of the high absorption loss of silicon dioxide (SiO_2) material above $\lambda \sim 3.6$ μm, moving to the mid-infrared (mid-IR) wavelength range is difficult within the silicon-on-insulator (SOI) technology. Consequently, for longer wavelength ranges, alternative materials or free-standing membrane structures have to be used.

Research dedicated to refractive index (RI) -based photonic sensors has increased in recent years, with most of these researches aiming at engineering new structures suitable for detection of a wide range of physical parameters, such as pressure or temperature. In particular, PhC cavities and waveguides structures have gained considerable attention for applications in biosensing [2, 3, 4]. In Ref. [2], a biosensor device is designed for detection of protein-concentrations and concentrations around 10 $\mu g/ml$ are measured with excellent signal to noise ratio. On the other hand, coating the internal surface of two-dimensional PhC microcavities with proteins of different sizes produces a different amount of resonance redshift and a molecule monolayer was detected with a total mass as small as 2.5 fg [3]. A new biosensor concept incorporating photonic crystal surface modes to sense small refractive index changes was designed [4]. In this work, a strongly confined mode interacted with the active medium while propagating along a PhC-air interface. The detection sensitivity for silicon PhC cavities was also improved by introducing multiple-hole defects (MHDs) in order to increase the surface area available for label-free detection without degrading the cavity quality factor [5, 6].

In another direction, an increasing number of works was devoted to hollow core slotted waveguides in the telecom range for their specific mode confinement

properties [7, 8, 9, 10, 11]. Several slotted photonic crystal geometries have been proposed to demonstrate cavities with high quality factors (Q) for uses in chemical and gas sensing in the near-IR telecom wavelengths near $\lambda = 1.55\ \mu m$ [12, 13, 14, 15, 16]. On the contrary, few works have been devoted for now to silicon slotted waveguides for sensing applications in the Mid-IR. Among recent works dealing with that objective, the transmission characteristics of slotted photonic crystal waveguides (SPCWs) suspended on a silicon-on-sapphire substrate was demonstrated experimentally at $\lambda = 3.43\ \mu m$ in Ref. [8]. In order to minimize the optical absorption path length and achieve high sensitivity in on-chip optical absorption spectroscopy, slotted photonic crystal structures, were also investigated in [17, 18]. In this work, the objective was to achieve the selective detection of volatile organic compounds [17] and greenhouse gases [18] using a 300 μm long SPCW absorption spectrometer which was demonstrated experimentally in the near-infrared wavelength range [17, 18]. Moreover, a new type of integrated optical sensor that performed sensing in mid-infrared spectrum range was designed in Ref. [19]. In the proposed configuration, a strong light confinement and interaction were obtained by engineering the structural parameters of square-lattice photonic crystal incorporated with a T-shaped air-slot. The direct interaction between the slot waveguide mode and the analyte infiltrated into the slot gave rise to an average refractive index sensitivity of 530 nm/RIU within the 1.10-1.25 index range and an average sensitivity of 390 nm/RIU between $n = 1.00$ and $n = 1.30$.

In this context, we design in this paper a mid-IR refractive index sensor with a higher sensitivity and a lower insertion loss level through numerical electromagnetic simulation. The device is made of an SPCW, which is formed by uniformly etching a rectangular nano-scale slot with air along the center of the line defect of a photonic crystal waveguide. An approach based on a resonant coupling mechanism is used to improve the coupling efficiency of the device [20]. For the set of optimized geometrical parameters, an SPCW with an average on-chip coupling loss of $-0.3\ dB$ over a 350 nm per interface is designed. Using plane wave (PW) calculations of photonic bands and finite-difference time-domain

(FDTD) simulations, both in 3D, the optical sensitivity of the proposed sensor is investigated in both the spectral and spatial domains by considering the infiltration of liquids. The sensitivity of the SPCW waveguide sensor is enhanced by fine-tuning the radius of the first row of the air holes near the air slot. A high-sensitivity liquid sensing device based on the optimized SPCW is then proposed and a sensitivity of ~ 1150 (nm/RIU) is obtained at $\lambda = 3.6$ μm. With respect to previous works, we bring here a viable design of Mid-IR slot photonic crystal waveguide sensors with beyond 1000 nm/RIU sensitivities and below -0.3 dB insertion loss.

2. Design of the slot waveguide configuration

To demonstrate mid-IR sensing, a slab photonic crystal waveguide (PCW) structure has been chosen, consisting of a two-dimensional hexagonal PhC lattice of the air holes etched in a silicon membrane. The slotted PCW was formed by omitting the central row of air holes in the ΓK direction and replacing it with a narrow air slot (see Fig. 1). A width of the air slot $W_{slot} = 0.33a$, a membrane thickness of $h = 0.48a$, and a radius of the air hole of $r_o = 0.29a$, where a is the lattice constant, were considered, respectively. The refractive index of the silicon membrane at the mid-infrared range was set to $n_{Si} = 3.42$. The lattice constant was set to $a = 1060$ nm, fixing the cut-off wavelength of the guided mode to about 3.6 μm, as shown hereafter. Three-dimensional plane wave expansion (3D-PWE) calculations were achieved to analyze the dispersion properties of the SPCW. This analysis was conducted by choosing a suitable supercell using the MPB software [21].

As described in previous works, if compared with standard W1 waveguides, the effect of the slot is to shift every guided modes of the photonic crystal waveguide towards higher frequencies and to pull the fundamental mode into the gap [9]. We recovered these classical trends and observed in the studied configuration the appearance of two optical modes remaining in the bulk photonic crystal bandgap, the so-called true-slot mode and the Ey-odd mode, respecti-

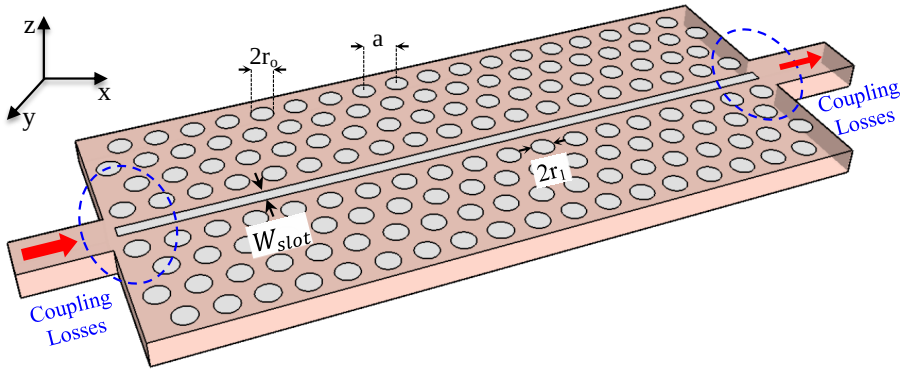

FIGURE 1: Schematic of the slotted photonic crystal waveguide (SPCW) where r is the radius of the air holes, a is the lattice constant, W_{slot} is the width of the air slot, h is the thickness of slab, and r_1 is the radius of the first row of the air holes.

vely (see Fig. 2). All the design steps described hereafter in this article were thus achieved by considering the first one only due to the field asymmetry of the Ey-odd mode one (see Fig. 2). As also visible in Fig. 2, the true-slot mode concentrates a non-negligible part of the propagating energy in the slot, which evidently is a good point for refractive index sensing purpose. Last, we also observe its slow light properties close to the edge of the Brillouin zone, graphically visible by its flat-band dispersion curve above $ka/2\pi = 0.45$. In terms of light-matter interaction, slow light propagation, i.e. large group index propagation, was reported to reinforce most of physical effects [7, 10, 11, 22], showing that the chosen configuration provided a suitable starting point for sensing purpose. Overall, these preliminary calculations thus provided a firm starting basis for the investigation of the device sensing properties.

3. Investigation of the sensing properties of the selected geometry

3.1. Improved coupling efficiency of the SPCW for refractive index sensing

As mentioned earlier, our main goal was to design an SPCW sensor with high sensitivity. However, the ability to efficiently couple light into the slow light

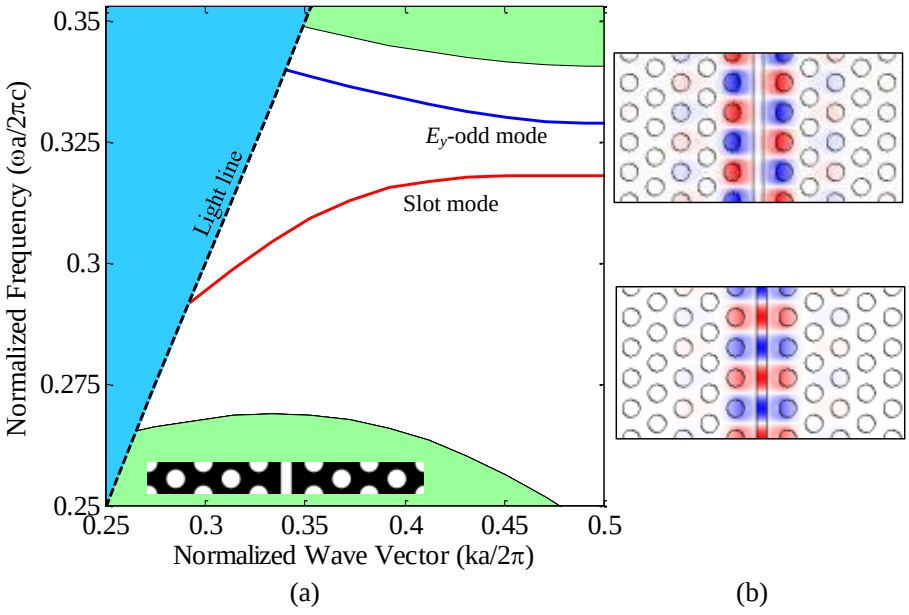

FIGURE 2: (a) The dispersion diagram of the SPCW, where the blue line indicates the Ey-odd mode, the red line indicates the slot mode, and the dotted line indicates the light line. (b) The Ey electric field component distribution of the Ey-odd mode and the slot mode at $k_x = 0.5\ (2\pi/a)$.

regime is a critical factor that may affect the performances of SPCW for practical applications. Recently, an effective method was proposed by adding suitable resonant couplers on both ends of the SPCW to improve the light coupling efficiency from a conventional strip waveguide into a SPCW (see Fig. 3(a)) [20]. Based on this structure, low coupling losses were realized experimentally. These coupling losses were as low as 1.5 dB per interface over a bandwidth of 78 nm around $\lambda = 1550\ nm$ [20]. Furthermore, this method proved to be robust in terms of fabrication. Consequently, we have adopted a similar strategy while transposing it to Mid-IR wavelengths.

The performance of the resonant coupler depends on several geometrical parameters, namely, the distance between the PhC edge and the edge of the slot (S), the width of the access waveguide (W), and the radius of the holes (R).

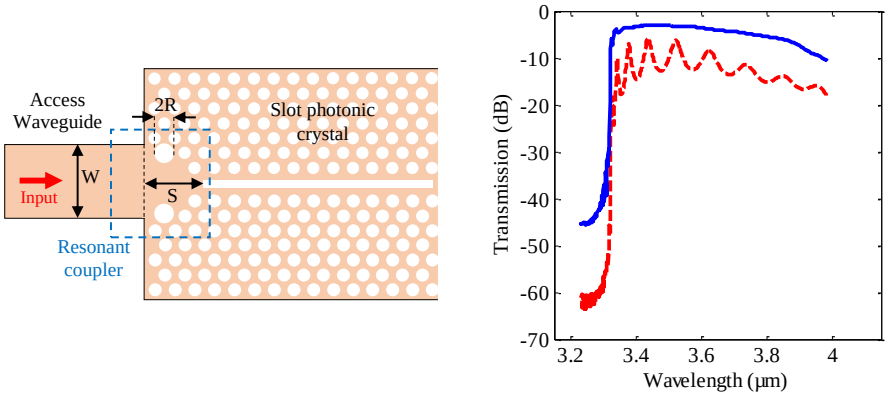

FIGURE 3: (a). Structure of SPCW with resonant structure added on both ends of the waveguide. The optimized parameters are : $R = 550\ nm$, $S = 3050\ nm$ and $W = 5200\ nm$. (b) Transmission spectrum of SPCW with (blue line) and without (dotted red line) a resonant coupling structure. The average coupling efficiency per interface in the 3350-3700 nm wavelength windows is $-0.3\ dB$ for the optimized structure.

A sketch of the geometry highlighting these different parameters is shown in Fig. 3(a). It was found that the distance slot (S) had the strongest effect on the transmission spectrum [20]. The properties of the SPCW with the resonant coupler were numerically simulated using a three-dimensional finite difference time-domain (3D-FDTD) method [23] using the MEEP software with subpixel smoothing for increased accuracy [24]. In order to prevent reflections, the simulation area was surrounded by a one-spatial unit thick perfectly matched layers absorbing out-going fields from the simulated region. In our 3D-FDTD calculation, the spatial resolution was set to 20 (namely, with a grid spacing of $a/20$, where a is the lattice constant). The S distance was then varied with 150 nm steps from $S = 2200$ to $S = 3500\ nm$. The defect radius was varied in 50 nm steps from $R = 400$ to $R = 550\ nm$, and the access width was varied in 200 nm steps from $W = 2000$ to $W = 6500\ nm$. The best found parameters of the resonant coupler were finally : $R = 550\ nm$, $S = 3050\ nm$ and $W = 5200\ nm$. Figure 3(b) shows the transmission spectrum of the SPCW structure after a

resonant coupler was added with optimized parameters. The equivalent transmission spectrum of the same SPCW without the resonant coupler is also shown for comparison. As visible, a nearly flat transmission spectrum with a $-0.3\ dB$ enhancement over a 350 nm bandwidth was achieved after optimization. The increase in efficiency of the light coupling for the proposed SPCW sensor is explained as follows : by inserting the defects at the ends of the SPCWs, the interference between multiple beams could produce a self-collimated beaming effect [20]. A high transmission spectrum with low level ripples was evidently achieved.

3.2. Sensing characteristics of a first SPCW configuration

The sensing properties of the SPCW structure were investigated by monitoring the evolution of the cut-off wavelength position resulting from the filling of the air holes by various refractive index liquids. To obtain a sufficient degree of consistency with a realistic structure, the transmission characteristics of the SPCW sensor were directly computed with 3D-FDTD. To study the performance of the proposed sensor, four liquids, namely, pentane, C_5H_{12} ($n_{clad} = 1.3570$); ethanol, C_2H_5OH ($n_{clad} = 1.3811$); octane, C_8H_{18} ($_{nclad}$= 1.4170); and ethylene glycol, $C_2H_6O_2$ ($n_{clad} = 1.4418$) were considered. The refractive index of each liquid was selected for the mid-IR wavelength range around $\lambda = 3.6\ m$. Figure 4(a) shows the evolution of the TE-like true slot mode transmission spectrum as a function of different refractive indices ranging from $n = 1.00$ to $n = 1.50$. As it can be anticipated, with the increase of RI of the liquids the transmission spectrum is shifted to longer wavelengths if compared with the situation of the SPCW structure immersed in air. Figure 4(b) shows the quantitative cut-off wavelength shift evolution versus the cover refractive index. A nearly linear shift is observed. A cut-off wavelength shift of $\sim 440\ nm$ is observed with a change in the local refractive index from $n_{clad} = 1.00$ (air) to $n_{clad} = 1.4418$ (ethylene glycol). The SPCW structure sensitivity ($S_\lambda = \partial\lambda/\partial n$) was further evaluated and estimated to $\sim 995\ nm/RIU$. In comparison with a silicon-based PhC waveguide with optimized radius of the first rows of air holes

nearest to the line-defect, which had a potential sensitivity of 282.4 nm/RIU at telecommunication wavelength [25], a comparatively much higher sensitivity of 995 nm/RIU is obtained in the present work.

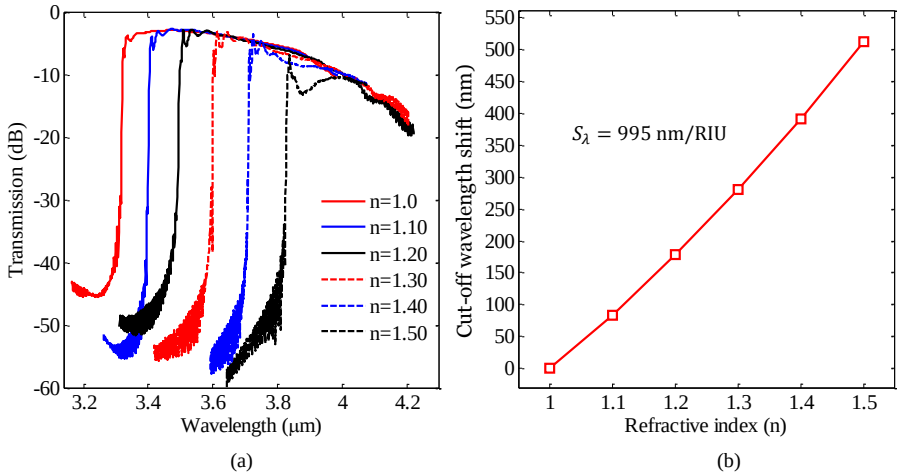

FIGURE 4: (a) Transmission spectra for TE-like polarization of the slotted photonic crystal waveguide studied in section 2 immersed into liquids with different refractive index ranging from $n = 1.0$ to $n = 1.50$ in 0.1 step. (b) The cut-off wavelength shifts for different refractive index values, giving rise to a sensitivity around 995 nm/RIU.

3.3. Improved sensing characteristics of the SPCW structure

As previously stated, the field of the slot mode of SPCW structure is very intense at the center of the slot. As a result, the modification of the first row of the air holes adjacent to the slot can lead to even strong light-matter interaction. In order to obtain higher sensitivities, we thus further optimized the proposed structure by enhancing the localization of the field in the SPCW structure through the tuning of the diameter of the first row of air holes (r_1) of the structure. Figure 5(a) shows the evolution of the dispersion curve for (r_1) ranging from $0.29a$ to $0.34a$, with a step of 0.01, while keeping other structural parameters unchanged with respect to those of the initial structure. It is seen that as the hole radius (r_1) is increased, the dispersion curve shifts toward higher fre-

quencies. This shift occurs due to the increase of the low dielectric permittivity material of the waveguide. Figure 5(b) illustrates the related variation in the edge frequency. As can be seen, the edge frequency linearly increases with the increasing (r_1) values.

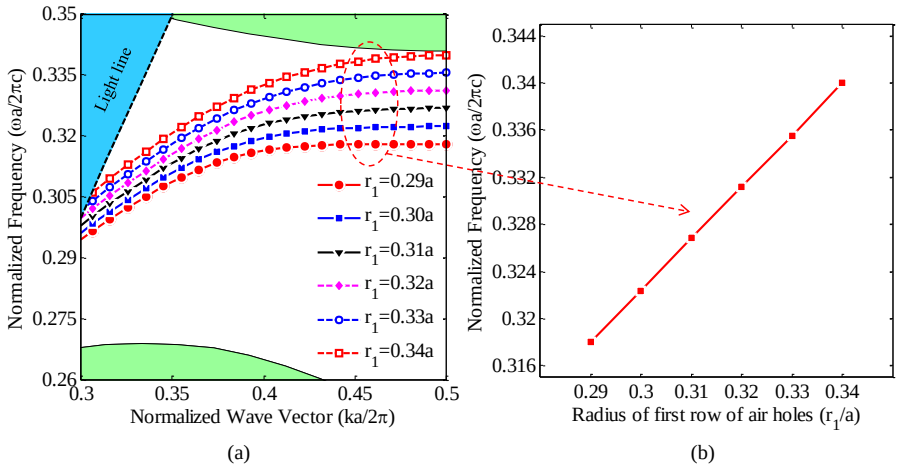

FIGURE 5: (a) TE-like band dispersion diagram for the slotted photonic crystal waveguide (SPCW) with different radiuses of the first row of the air holes ranging from $r_1 = 0.29a$ to $r_1 = 0.34a$ in 0.01 step. (b) The SPCW band edge frequency versus the hole radius r_1.

Using a similar approach, the refractive index sensitivities of the modified SPCW structures were studied through 3D-FDTD simulations. Figure 6(a) shows the variation in the cut-off wavelength shift of the SPCW structure as a function of the refractive index of the infiltrated liquids for different (r_1) values. As visible, a linear relationship between the cut-off wavelength shift and the refractive of the cladding liquids is obtained and a slight optimization of the device sensitivity can be obtained by this approach. The best result was obtained for $r_1 = 360\ nm$. The highest shift for a cut-off wavelength of 510 nm was obtained based on this (r_1) value. Figure 6(b) shows the corresponding sensitivity curve of the sensing device as a function of the hole radius (r_1). It can be seen that, as the radius r_1 increases, the sensitivity values show an ascending trend up to $r_1 = 360\ nm$. The highest sensitivity is obtained as $S_\lambda = 1150\ nm/RIU$

for the infiltration of ethylene glycol. In light of the literature on photonic crystal waveguides sensors, these calculations indicate that the designed sensor has a strong potential for refractive index sensing in the mid-infrared wavelength range.

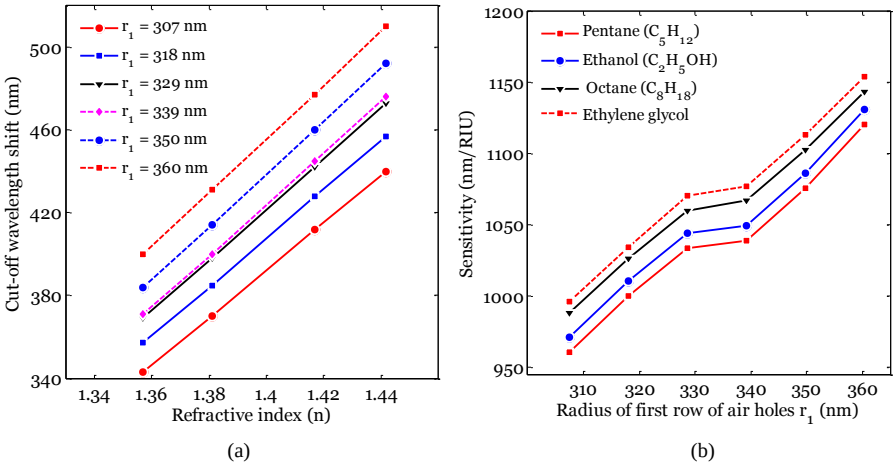

FIGURE 6: (a) Variation of the cut-off wavelength shift as a function of the refractive indices for the different radiuses of the first row of the air holes (r_1). (b) Variation of the sensitivity as a function of the radius of the first row of air holes for different refractive indices of the liquids.

4. Conclusion

In this article, we have explored the possibility of transposing concepts derived from telecom-range silicon photon devices based on photonic crystal slot waveguides for the realization of refractive index sensors around $\lambda = 3.6\ m$. An advantage of this approach is that the fabrication of periodic structures is simpler in the mid-infrared wavelength in view of the relaxed lithography constraints. The approach proposed in this article, based on a particular configuration, thus opens the way to a whole range of photonic crystal structures whose transposition from the telecom domain to the mid-IR domain is effective

in terms of possible exploitation of physical effects. We have considered completely liberated silicon structures, i.e. free standing membrane ones, and explored the sensitivity of slot photonic crystal slow light true slot modes to cladding refractive index variation. A specific effort was devoted to the engineering of a resonant coupling stage to sustain the practical viability of photonic crystal silicon refractive index sensing structures for applications. Moreover, all numerical calculations were carried out using realistic 3D electromagnetic simulation.

A high-sensitivity beyond 1000 nm/RIU was demonstrated at $\lambda = 3.6\ m$ ($S_\lambda = 1150\ nm/RIU$ in the best optimized case) for a device of 22.3 μm total length. These very encouraging results also show that the whole range of photonic crystal cavities toolbox can be envisaged for the realization of refractive index sensors in the mid-IR.

References

[1] R. Soref, Mid-infrared photonics in silicon and germanium, Nature photonics 4 (8) (2010) 495–497.

[2] N. Skivesen, A. Têtu, M. Kristensen, J. Kjems, L. H. Frandsen, P. I. Borel, Photonic-crystal waveguide biosensor, Optics Express 15 (6) (2007) 3169–3176.

[3] M. Lee, P. M. Fauchet, Two-dimensional silicon photonic crystal based biosensing platform for protein detection, Optics express 15 (8) (2007) 4530–4535.

[4] H. Kurt, M. N. Erim, N. Erim, Various photonic crystal bio-sensor configurations based on optical surface modes, Sensors and Actuators B : Chemical 165 (1) (2012) 68–75.

[5] C. Kang, C. T. Phare, Y. A. Vlasov, S. Assefa, S. M. Weiss, Photonic crystal slab sensor with enhanced surface area, Optics express 18 (26) (2010) 27930–27937.

[6] C. Kang, S. M. Weiss, Photonic crystal with multiple-hole defect for sensor applications, Optics express 16 (22) (2008) 18188–18193.

[7] Y.-n. Zhang, Y. Zhao, Q. Wang, Optimizing the slow light properties of slotted photonic crystal waveguide and its application in a high-sensitivity gas sensing system, Measurement Science and Technology 24 (10) (2013) 105109.

[8] Y. Zou, S. Chakravarty, P. Wray, R. T. Chen, Mid-infrared holey and slotted photonic crystal waveguides in silicon-on-sapphire for chemical warfare simulant detection, Sensors and Actuators B : Chemical 221 (2015) 1094–1103.

[9] A. Di Falco, L. OFaolain, T. Krauss, Photonic crystal slotted slab waveguides, Photonics and Nanostructures-Fundamentals and Applications 6 (1) (2008) 38–41.

[10] C. Caer, X. Le Roux, D. Marris-Morini, N. Izard, L. Vivien, D. Gao, E. Cassan, et al., Dispersion engineering of wide slot photonic crystal waveguides by bragg-like corrugation of the slot, IEEE Photonics Technology Letters 23 (18) (2011) 1298–1300.

[11] C. Caer, X. Le Roux, E. Cassan, Enhanced localization of light in slow wave slot photonic crystal waveguides, Optics letters 37 (17) (2012) 3660–3662.

[12] A. Di Falco, L. OFaolain, T. Krauss, Chemical sensing in slotted photonic crystal heterostructure cavities, Applied physics letters 94 (6) (2009) 063503.

[13] T. Yamamoto, M. Notomi, H. Taniyama, E. Kuramochi, Y. Yoshikawa, Y. Torii, T. Kuga, Design of a high-q air-slot cavity based on a width-modulated line-defect in a photonic crystal slab, Optics express 16 (18) (2008) 13809–13817.

[14] J. Gao, J. F. McMillan, M.-C. Wu, J. Zheng, S. Assefa, C. W. Wong, Demonstration of an air-slot mode-gap confined photonic crystal slab nanoca-

vity with ultrasmall mode volumes, Applied Physics Letters 96 (5) (2010) 051123.

[15] S.-H. Kwon, T. Sünner, M. Kamp, A. Forchel, Optimization of photonic crystal cavity for chemical sensing, Optics Express 16 (16) (2008) 11709–11717.

[16] J. Jágerská, H. Zhang, Z. Diao, N. Le Thomas, R. Houdré, Refractive index sensing with an air-slot photonic crystal nanocavity, Optics letters 35 (15) (2010) 2523–2525.

[17] W.-C. Lai, S. Chakravarty, X. Wang, C. Lin, R. T. Chen, Photonic crystal slot waveguide absorption spectrometer for on-chip near-infrared spectroscopy of xylene in water, Applied Physics Letters 98 (2) (2011) 7.

[18] W.-C. Lai, S. Chakravarty, X. Wang, C. Lin, R. T. Chen, On-chip methane sensing by near-ir absorption signatures in a photonic crystal slot waveguide, Optics letters 36 (6) (2011) 984–986.

[19] M. Turduev, I. H. Giden, C. Babayiğit, Z. Hayran, E. Bor, Ç. Boztuğ, H. Kurt, K. Staliunas, Mid-infrared t-shaped photonic crystal waveguide for optical refractive index sensing, Sensors and Actuators B : Chemical 245 (2017) 765–773.

[20] M. Scullion, T. Krauss, A. Di Falco, High efficiency interface for coupling into slotted photonic crystal waveguides, IEEE Photonics Journal 3 (2) (2011) 203–208.

[21] S. G. Johnson, J. D. Joannopoulos, Block-iterative frequency-domain methods for maxwells equations in a planewave basis, Optics express 8 (3) (2001) 173–190.

[22] N. A. Mortensen, S. Xiao, J. Pedersen, Liquid-infiltrated photonic crystals : enhanced light-matter interactions for lab-on-a-chip applications, Microfluidics and Nanofluidics 4 (1-2) (2008) 117–127.

[23] A. Taflove, S. C. Hagness, Computational electrodynamics, Artech house, 2005.

[24] A. F. Oskooi, D. Roundy, M. Ibanescu, P. Bermel, J. D. Joannopoulos, S. G. Johnson, Meep : A flexible free-software package for electromagnetic simulations by the fdtd method, Computer Physics Communications 181 (3) (2010) 687–702.

[25] F. Bagci, B. Akaoglu, Enhancement of refractive index sensitivity in photonic crystal waveguide based sensors by selective infiltration, Acta Physica Polonica A 124 (1) (2013) 50–55.